*Korean J. Chem. Eng.*, 36(9), 1482-1488 (2019)
DOI: 10.1007/s11814-019-0346-3

pISSN: 0256-1115
eISSN: 1975-7220

# Mesoporous carbon supported MgO for $CO_2$ capture and separation of $CO_2/N_2$

**Harshitha Burri*, Rumana Anjum*, Ramesh Babu Gurram**, Harisekhar Mitta***, Suresh Mutyala****, and Madhavi Jonnalagadda*,†**

*Department of Chemistry, Government Degree College for Women, Karimnagar, Telangana, India
**Catalysis Laboratory, Indian Institute of Chemical Technology, Hyderabad-500007, India
***State Key Laboratory of Catalysis, Dalian Institute of Chemical Physics,
Chinese Academy of Science, Dalian-116023, China
****Department of Chemistry and Key Laboratory for Preparation and Application of Ordered Structural Materials
of Guangdong Province, Shantou University, Guangdong 515063, China
(*Received 3 February 2019 • accepted 23 July 2019*)

**Abstract**−Mesoporous carbon derived from pongamia pinnata fruit hulls was used as support to incorporate magnesium oxide for the study of $CO_2$ adsorption and separation of $CO_2/N_2$. All synthesized adsorbents were characterized by PXRD, $N_2$ adsorption-desorption isotherms, Raman and SEM with EDX techniques. Characterization results revealed the existence of magnesium oxide on mesoporous carbon. $CO_2$ adsorption on MgO incorporated mesoporous carbon was higher than bulk mesoporous carbon, due to the electrostatic interaction between magnesium oxide and $CO_2$. High $CO_2$ adsorption capacity 1.68 mmol/g was obtained for 10 wt% MgO incorporated mesoporous carbon at 298 K, 1 bar compared to remaining loadings, because of the high content of MgO. However, the $N_2$ adsorption capacity decreased with the increase of MgO content due to a decrease in surface area and no interaction of the $N_2$ molecule with the adsorbent. The selectivity of $CO_2/N_2$ was higher on 10 wt% MgO incorporated mesoporous carbon and the value was 40. The heat of $CO_2$ adsorption was 36 KJ/mol at low coverage of $CO_2$, and $CO_2$ adsorption capacity was constant in each adsorption cycle over the same adsorbent.

Keywords: MgO, Mesoporous Carbon, $CO_2$ and $N_2$ Adsorption, Selectivity, Heat of $CO_2$ Adsorption

## INTRODUCTION

Carbon dioxide is one of the environmental pollutant gases causing global warming. It is produced by the consumption of fossil fuel, high growth of petrochemical, automobile industries, and power plants [1]. $CO_2$ concentration can be minimized by the development of an alternative energy source until commercial energy sources have to use for the production of energy. Carbon dioxide in the atmosphere can be reduced by carbon capture and separation. In power plants, a large amount of $CO_2$ is liberated that is absorbed by the use of liquid amine solutions. However, a large amount of energy is required for the regeneration, and volatile organic compounds are liberated which damage the pipeline system [2]. Adsorption is one of the best techniques to reduce the concentration of $CO_2$. In this process, energy consumption and damage to the pipeline system are less. So far, commercially available carbon materials [3], zeolites [4], clays [5] and silica materials [6] have been used for $CO_2$ capture and separation.

Activated carbon is one of the most abundant carbon materials [7]. However, large-scale synthesis is hindered because of the non-renewable source. Porous carbon was synthesized from renewable sources such as waste tea [8], coffee grounds [9], cotton stalk [10], peach stone and olive stone [11,12], biodiesel solid residue [13] and rice husk [14]. Pongamia pinnata fruit hulls are also a source for the porous carbon synthesis. Bio-oil is produced from pongamia pinnata seeds. During the production of bio-oil, pongamia pinnata fruit hulls are thrown without any commercial use. From the fruit hulls, we have synthesized mesoporous carbon to capture $CO_2$. $CO_2$ adsorption capacity on mesoporous carbon can be enhanced by the incorporation of basic metal oxides, amine or heteroatom which generates basic sites to capture $CO_2$.

Iron oxide-doped MCM-41 has shown $CO_2$ adsorption capacity 0.87 mmol/g at 298 K, 1 bar [15]. $CeO_2$ incorporated mesoporous carbon showed $CO_2$ adsorption 1.77 mmol/g at 303 K, 1 bar [16]. $Cu_2O$ and NiO incorporated porous carbon showed high $CO_2$ adsorption capacity compared to bulk porous carbon [17,18]. S-doped microporous carbon has shown 3.7 mmol/g of $CO_2$ adsorption at 298 K, 1 bar [19]. N-enriched activated carbon from Procambarus Clarkii shells has shown 2.55 mmol/g of $CO_2$ adsorption at 298 K, 1 bar [20]. MgO modified mesoporous silica has shown 1.34 mmol/g of $CO_2$ at 303 K [21]. Similarly, MgO supported titanium oxide showed 0.48 mmol/g of $CO_2$ adsorption at 298 K [22]. In all reported adsorbents, the $CO_2$ adsorption capacity was higher due to electrostatic interaction between a metal oxide and $CO_2$. In this article, we studied $CO_2$ adsorption on mesoporous carbon and magnesium oxide incorporated mesoporous carbon in low pressure at 298 K. Moreover, the selectivity of $CO_2/N_2$, the heat of $CO_2$ adsorption and multiple $CO_2$ adsorption cycles was studied.

†To whom correspondence should be addressed.
E-mail: madhavi0521@gmail.com

## EXPERIMENTAL

### 1. Materials

All analytical grade chemicals such as magnesium nitrate hexahydrate ($Mg(NO_3)_2{\cdot}6H_2O$), Orthophosphoric acid ($H_3PO_4$) were purchased from all commercial sources and used without further purification. Laboratory purified double distilled water was used for the synthesis of adsorbents. Ultra-high pure gases such as helium, carbon dioxide, nitrogen were purchased from local suppliers in India.

### 2. Synthesis of Adsorbents

Pongamia pinnata fruit hulls were collected from the forest region of Telangana, India. The fruit hulls were dried and crushed into a fine powder, then chemically activated using orthophosphoric acid with 1 : 1 (w/w%) followed by drying at 100 °C for 12 h, then calcined at 723 K for 4 h in a nitrogen atmosphere. The obtained product was washed with distilled water until neutral pH was obtained, then vacuum dried at 373 K for 12 h. Finally, we got mesoporous carbon [23]; it was denoted as MC. Magnesium oxide incorporated mesoporous carbon was synthesized by the impregnation method. The desired quantity of magnesium nitrate hexahydrate was dissolved in 10 mL distilled water, then 1 g of mesoporous carbon was added to it. The mixture was stirred at room temperature for 1 h, then dried at 373 K for 12 h. The dried product was calcined at 723 K for 4 h in the nitrogen atmosphere. Finally, we got magnesium oxide incorporated mesoporous carbon; it was denoted as xMgO/MC, where x represents the weight percentage of magnesium oxide (x=2, 5 and 10).

### 3. Characterization

Powdered X-ray diffraction patterns were recorded on Rigaku MiniFlex600 X-ray diffractometer using Ni-filtered Cu $K_\alpha$ radiation ($\lambda$=1.54 A°) in the scan range $2\theta$=10-80°. $N_2$ adsorption-desorption isotherms were measured using Micromeritics ASAP 2020 surface area and porosity analyzer at 77 K. Prior to adsorption study, about 0.1 g of sample was degasified at 473 K for 4 h under vacuum. The specific surface area was calculated by the BET method. Total pore volume at a relative pressure of 0.99 and micropore volume by the t-plot method was calculated from $N_2$ adsorption-desorption isotherms. Raman spectra were recorded using LabRAM HR800 Raman spectrometer having laser wavelength 514 nm. Morphological image with metal composition was obtained from ZEISS Sigma 300 Scanning electron microscope analyzer.

### 4. $CO_2$ and $N_2$ Adsorption Measurement

$CO_2$ and $N_2$ adsorption isotherms were measured on Micromeritics ASAP 2020 analyzer at low pressure 0-100 kPa at 298 K. Sample temperature was controlled by the thermostatic bath which was connected to water circulating jacket. Free space of the sample was measured using helium gas. About 0.1 g of sample was degasified similar to $N_2$ adsorption-desorption isotherm measurement at 77 K, then cooled to room temperature for the study of $CO_2$ and $N_2$ adsorption isotherms. The selectivity of $CO_2/N_2$ was calculated using the initial slope of each isotherm by Henry's Law. The heat of $CO_2$ adsorption was calculated by the Clausius-Clapeyron equation using adsorption isotherms measured at 283, 298 and 303 K. Multiple $CO_2$ adsorption cycles were also carried out, after desorbing adsorbed $CO_2$ at 473 K for 2 h under vacuum.

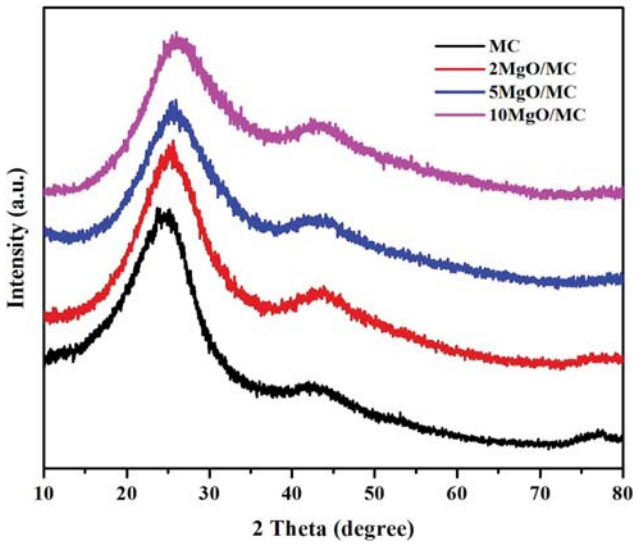


**Fig. 1. XRD patterns of MC and MgO incorporated MC.**

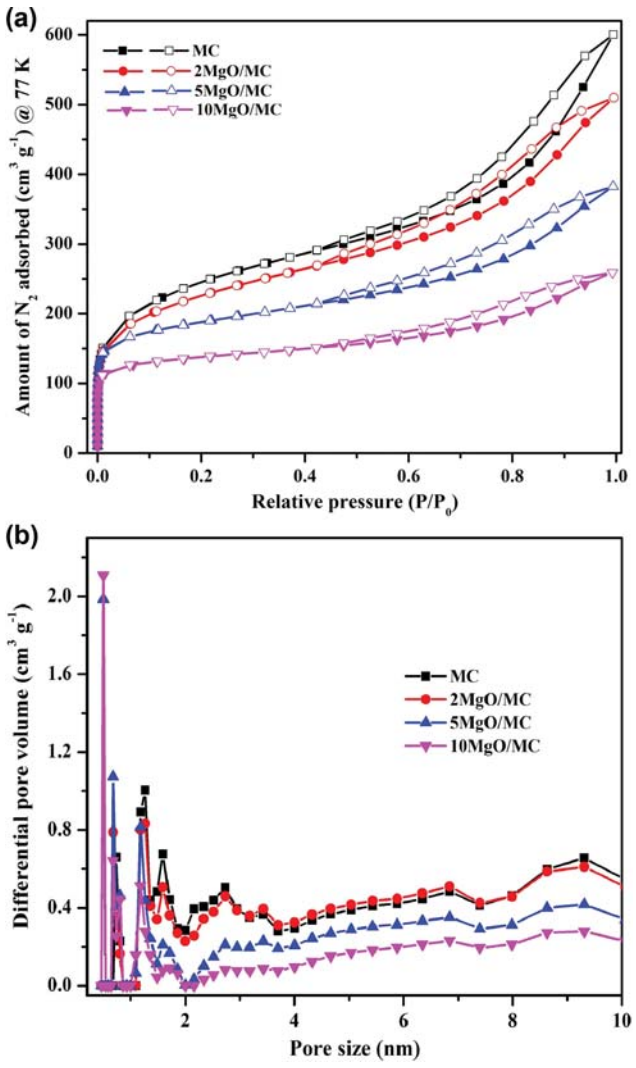


**Fig. 2. (a) $N_2$ adsorption-desorption isotherms and (b) pore size distribution of MC and MgO incorporated MC.**

## RESULTS AND DISCUSSION

The X-ray diffraction pattern of mesoporous carbon and MgO incorporated mesoporous carbon samples are shown in Fig. 1. MC shows two broad diffraction peaks at $2\theta$=24.2° and 43.66° having planes (002) and (100), respectively, which are characteristic peaks of mesoporous carbon [24]. Moreover, MgO incorporated mesoporous carbon samples also show diffraction peaks similar to mesoporous carbon and no diffraction peaks related to MgO appeared. It indicates that MgO was well-dispersed over mesoporous carbon. However, the intensity of major diffraction peaks of MC decreased with the increase of MgO loading and shifted towards higher angle. Similar results have been reported on nickel loaded MCM-41 for hydrogen storage [25].

From $N_2$ adsorption-desorption isotherm, the porosity of carbon material can be found. Fig. 2 shows $N_2$ adsorption-desorption isotherms of MC and MgO incorporated MC at 77 K. Textural properties are presented in Table 1. MC shows a large amount of $N_2$ uptake below the relative pressure of 0.1 and a hysteresis loop above the relative pressure of 0.4. The isotherm pattern of MC is similar to type-I and type-IV of classification of porous materials by IUPAC [26], which represent that MC has micro and mesopores. The specific surface area, total pore volume and pore size of MC were 840 $m^2$/g, 0.94 $cm^3$/g, and 4.4 nm, respectively. Similarly, MgO incorporated MC samples show the same isotherm pattern similar to MC. But, the amount of $N_2$ uptake is less. As the content of MgO increased, the amount of $N_2$ uptake was decreased. Hence, a change in textural properties has been observed. The specific surface area was decreased to 421 $m^2$/g, the total pore volume 0.34 $cm^3$/g and pore size 3.8 nm. However, micropore surface area and micropore volume were increased, which indicates that incorporated MgO has occupied mesopores of MC.

Raman analysis is used to determine the crystallinity of carbon material. Fig. 3 shows the Raman spectra of MC and 10MgO/MC. Mesoporous carbon shows two Raman bands at 1,325 $cm^{-1}$ and 1,580 $cm^{-1}$ which correspond to D-band and G-band, respectively [27]. D-band represents disordered carbon and G-band represents graphitic carbon. The ratio of the intensity of bands ($I_D/I_G$) represents the degree of graphitization. In mesoporous carbon, the intensity of G-band is higher than D-band. It represents that mesoporous carbon has a graphitic nature. The $I_D/I_G$ value was 0.95 for MC and 0.97 for 10MgO/MC. By incorporation of MgO, the graphitic nature of MC decreased [28]. Morphology with the elemental composition of MC and 10MgO/MC is shown in Fig. 4. MC shows irregular shaped carbon particles (Fig. 4(a)). Same morphology was replicated in 10 wt% MgO incorporated mesoporous carbon, which indicates that magnesium oxide was homogenously distributed over carbon surface (Fig. 4(b)). The amount of magnesium was calculated from EDX and the value was 4.92 wt%.

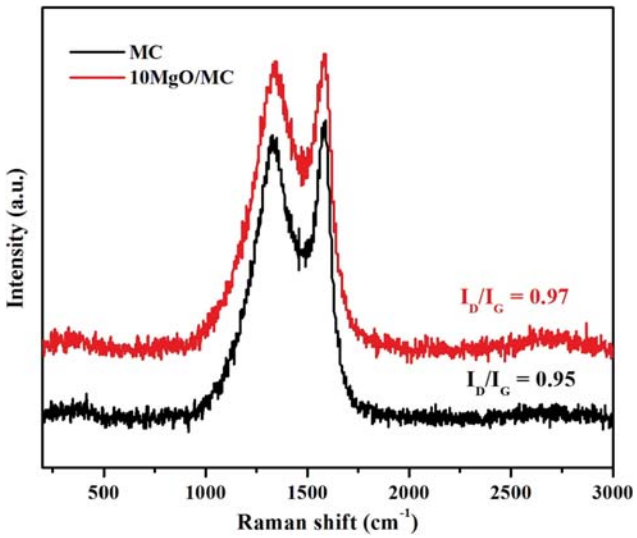


**Fig. 3. Raman spectra of MC and MgO incorporated MC.**

Fig. 5(a) shows single component adsorption isotherm of $CO_2$ on MC and MgO incorporated MC samples in low pressure at 298 K. With the increase of $CO_2$ pressure, the amount of $CO_2$ adsorption capacity was increased. $CO_2$ adsorption capacity was 0.9 mmol $g^{-1}$ for MC, 1.0 mmol $g^{-1}$ for 2MgO/MC, 1.5 mmol $g^{-1}$ for 5MgO/MC and 1.68 mmol $g^{-1}$ for 10MgO/MC at 298 K, 1 bar. The $CO_2$ adsorption capacity of MgO incorporated MC samples was higher compared to MC because of electrostatic interaction between MgO and $CO_2$. With the increase of MgO content, the amount of $CO_2$ adsorption capacity increased due to the high content of magnesium oxide. It could be confirmed by calculating the amount of

**Table 1. Textural properties of MC and MgO incorporated MC**

| Adsorbent | $S_{BET}$[a] ($m^2$ $g^{-1}$) | $S_{micro}$[b] ($m^2$ $g^{-1}$) | $V_{total}$[c] ($cm^3$ $g^{-1}$) | $V_{micro}$[d] ($cm^3$ $g^{-1}$) | $V_{meso}$[e] ($cm^3$ $g^{-1}$) | $V_{meso}$[f] (%) | Pore size[g] (nm) |
|---|---|---|---|---|---|---|---|
| MC | 840 | 225 | 0.93 | 0.11 | 0.82 | 88 | 4.4 |
| 2MgO/MC | 743 | 189 | 0.79 | 0.11 | 0.68 | 86 | 4.2 |
| 5MgO/MC | 591 | 293 | 0.59 | 0.16 | 0.43 | 73 | 4.0 |
| 10MgO/MC | 421 | 263 | 0.40 | 0.14 | 0.26 | 65 | 3.8 |

[a]Multipoint BET surface area
[b]Micropore surface area by t-plot
[c]Total pore volume at $P/P_0$=0.99
[d]Micropore volume by t-plot
[e]Mesopore volume=$V_{total}-V_{micro}$
[f]Mesopore volume (%)=$V_{meso}/V_{total}$
[g]Average pore size by BET method (4V/S.A)

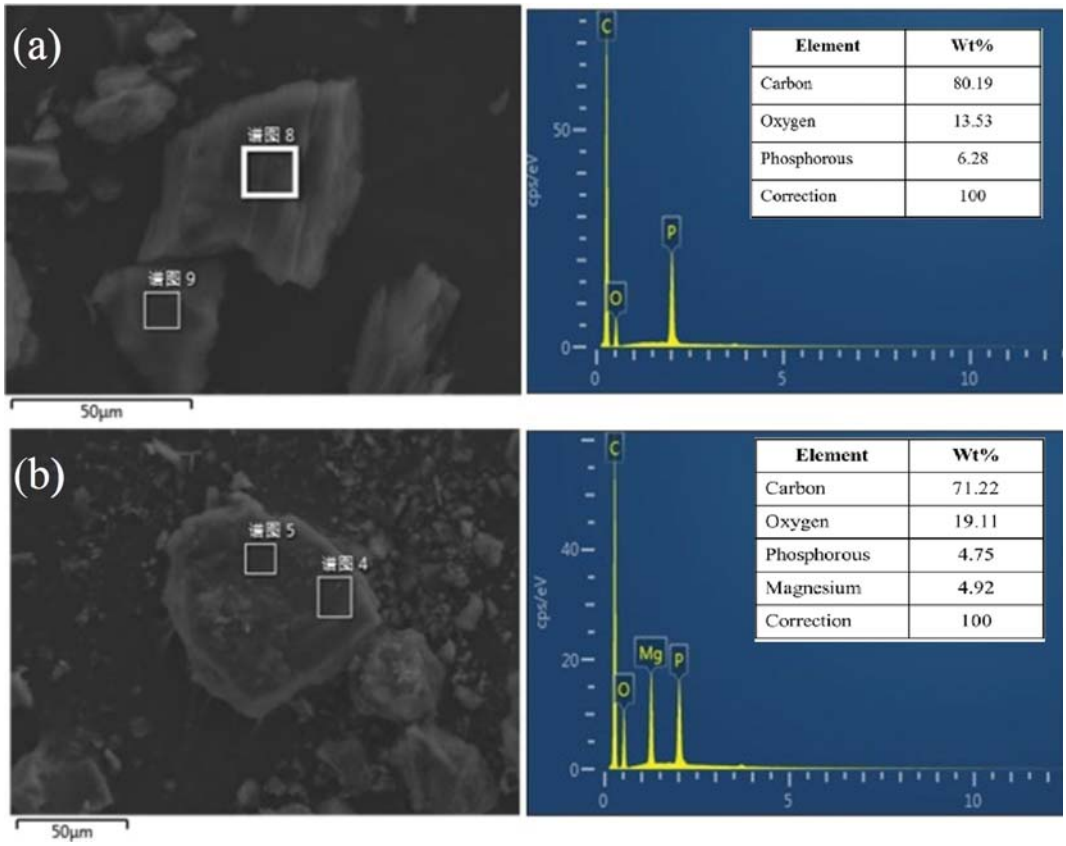


**Fig. 4. SEM with EDX of (a) MC and (b) 10MgO/MC.**

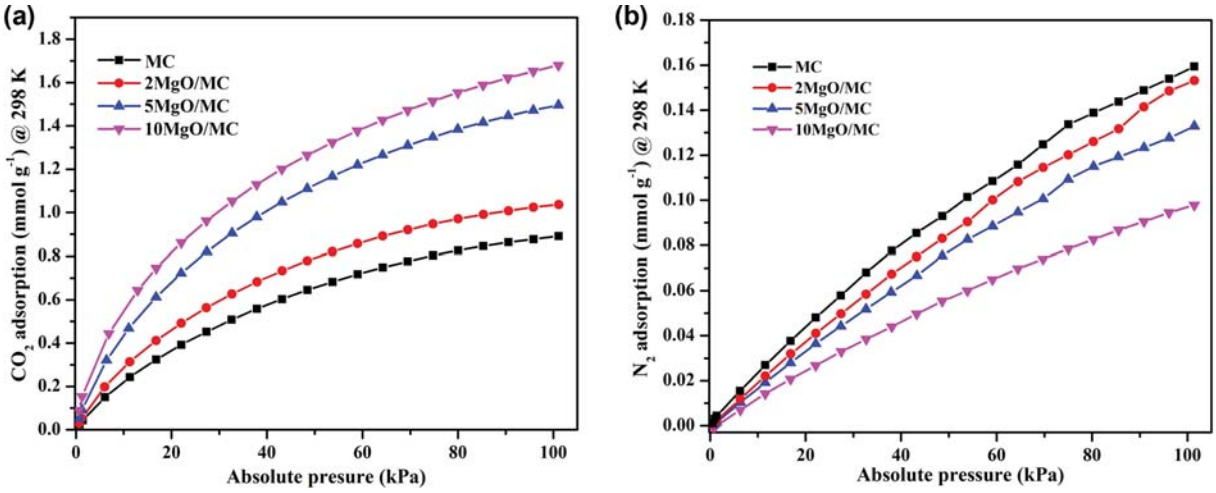


**Fig. 5. (a) $CO_2$ and (b) $N_2$ adsorption isotherms of MC and MgO incorporated MC at 298 K.**

$CO_2$ adsorption on unit surface area (Fig. 6(a)). $CO_2$ adsorption on the unit surface area of MgO incorporated mesoporous carbon samples was higher than porous carbon. Hence, $CO_2$ adsorption depends on the surface chemistry of the adsorbent instead of surface area. Fig. 5(b) shows $N_2$ adsorption of synthesized adsorbents under a similar condition of $CO_2$ adsorption. The $N_2$ adsorption capacity was 0.16 mmol $g^{-1}$ for MC, 0.15 mmol $g^{-1}$ for 2MgO/MC, 0.13 mmol $g^{-1}$ for 5MgO/MC and 0.09 mmol $g^{-1}$ for 10MgO/MC at 298 K, 1 bar. The decrease in $N_2$ adsorption capacity with the increase of MgO content was due to the decrease in surface area.

The difference in adsorption capacity of $CO_2$ and $N_2$ is helpful for studying the selectivity of $CO_2$ over $N_2$. In industrial flue gas, $CO_2$ is a major component gas, so it is essential to study the selectivity of $CO_2/N_2$. It was calculated using the initial slope of each isotherm in low pressure by Henry's law [29]. Fig. 6(b) shows the

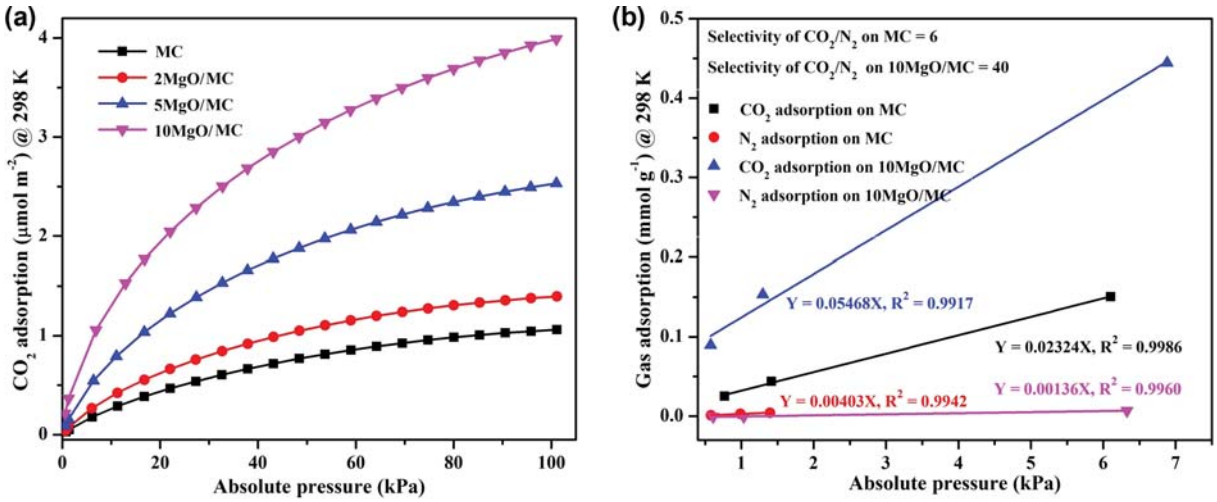


**Fig. 6. (a) $CO_2$ adsorption on unit surface area, (b) selectivity of $CO_2/N_2$ on MC and 10MgO/MC.**

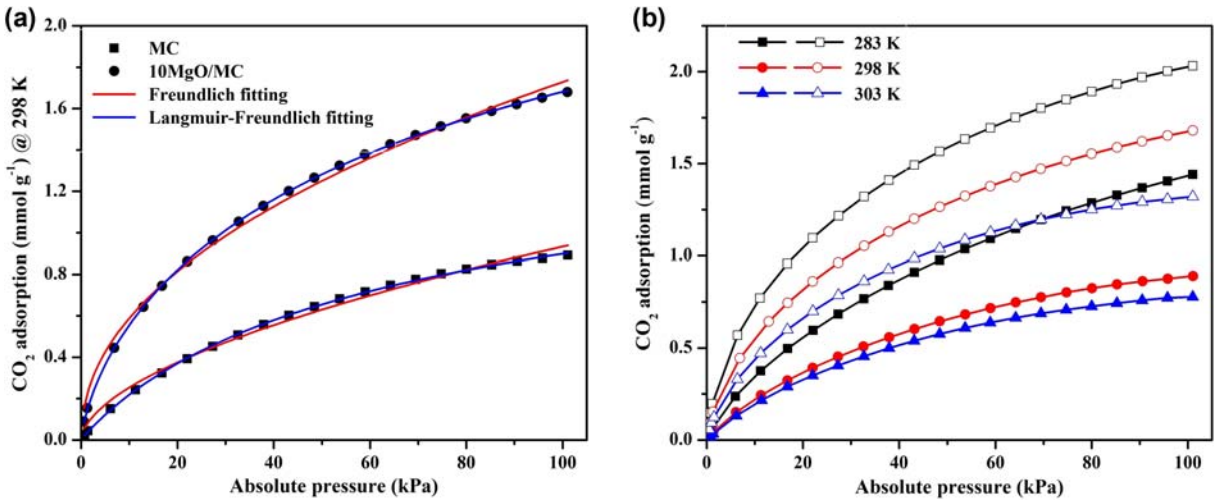


**Fig. 7. (a) Fitting curves of experimental $CO_2$ adsorption data (b) $CO_2$ adsorption of MC (closed symbol) and 10MgO/MC (open symbol) at different temperatures.**

**Table 2. Fitting parameters of Freundlich and Langmuir-Freundlich models**

| Adsorbent | Freundlich model | | | Langmuir-Freundlich model | | | |
|---|---|---|---|---|---|---|---|
| | $k_F$ ($kPa^{-1}$) | n | $R^2$ | $Q_{max}$ (mmol $g^{-1}$) | K ($kPa^{-1}$) | n | $R^2$ |
| MC | 0.0688 | 1.7666 | 0.9909 | 1.4988 | 0.0195 | 1.0609 | 0.9997 |
| 10MgO/MC | 0.2005 | 2.1378 | 0.9942 | 3.2968 | 0.0395 | 1.4077 | 0.9999 |

selectivity of $CO_2/N_2$ on MC and 10MgO/MC. The selectivity value was 6 for MC and 40 for 10MgO/MC. High selectivity value on 10MgO/MC was due to the high adsorption of $CO_2$. To describe the adsorption of $CO_2$ on the adsorbent, experimental $CO_2$ adsorption data of all synthesized adsorbents was fitted with Freundlich and Langmuir-Freundlich models [30]. These models can be expressed as follows.

$$\text{Freundlich model: } Q = k_F P^{1/n} \quad (1)$$

$$\text{Langmuir-Freundlich model: } Q = Q_{max}\frac{KP^{1/n}}{1+KP^{1/n}} \quad (2)$$

where Q is adsorption capacity at equilibrium in mmol/g, $Q_{max}$ is maximum adsorption capacity in mmol/g, P is pressure in kPa, $k_F$ and K are Freundlich, Langmuir-Freundlich coefficients and n is heterogeneity factor. Fitting curves of experimental $CO_2$ adsorption data of MC and 10MgO/MC are shown in Fig. 7(a) and fitting parameters are presented in Table 2. Langmuir-Freundlich model was well-fitted with experimental $CO_2$ adsorption data of both adsorbents with regression coefficient ($R^2$) higher than 0.999, and $Q_{max}$ was higher on 10MgO/MC.

The interaction between adsorbent and adsorbate can be known by calculating the heat of adsorption using the Clausius-Clapeyron

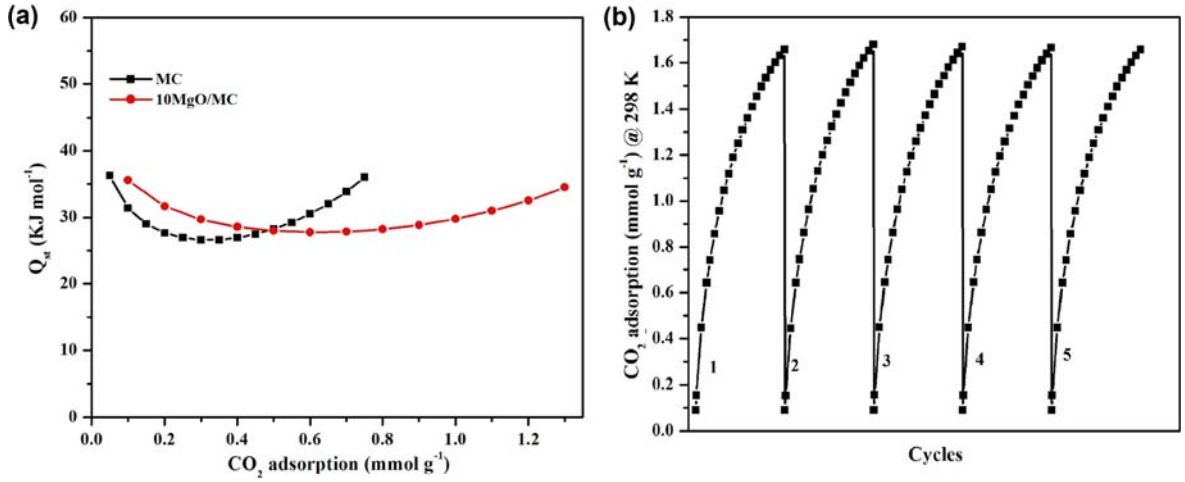


**Fig. 8. (a) Heat of $CO_2$ adsorption on MC and 10MgO/MC, (b) $CO_2$ adsorption cycles of 10MgO/MC at 298 K.**

**Table 3. Comparison of $CO_2$ adsorption capacity and selectivity with reported adsorbents**

| Adsorbent | $CO_2$ adsorption at 298 K, 1 bar (mmol g$^{-1}$) | Selectivity ($CO_2/N_2$) | Reference |
|---|---|---|---|
| NiO/mesoporous carbon | 2.02 (303 K) | 17.6 | [16] |
| $Fe_2O_3$ doped MCM-41 | 0.87 | - | [15] |
| Zeolite-13X | 1.70 | - | [32] |
| Karanja seed cake | 1.78 (343 K) | - | [33] |
| $MgO/Al_2O_3$ | 1.60 (333 K) | - | [34] |
| N-doped microporous carbon | 1.9 | 21 | [29] |
| MgO/mesoporous carbon | 1.68 | 40 | Present work |

equation [31]:

$$\ln P = \frac{-Q_{st}}{RT} + C$$

Here, P is pressure in kPa, T is the absolute temperature in K, R is universal gas constant (8.314 J/K·mol), C is constant and $Q_{st}$ is the heat of adsorption. The partial pressure at different temperatures for the fixed amount of gas uptake can be obtained from the Langmuir-Freundlich model. By drawing a graph between ln P versus 1/T with straight line fitting, we can obtain the slope. Finally, $Q_{st}$ was calculated from the slope. For the calculation of heat of $CO_2$ adsorption on MC and 10MgO/MC, we measured $CO_2$ adsorption at 283 K and 303 K also (see Fig. 7(b)). A decrease in $CO_2$ adsorption capacity was observed on both adsorbents with the increase of temperature. Fig. 8(a) shows the heat of $CO_2$ adsorption with gas adsorption capacity on MC and 10MgO/MC. The heat of $CO_2$ adsorption was 36.3-36.0 KJ/mole for MC and 36-34.5 KJ/mole for 10MgO/MC. At low coverage of $CO_2$, the heat of $CO_2$ adsorption for 10MgO/MC was higher than MC. It was due to the strong interaction between MgO and $CO_2$. The $Q_{st}$ was decreased to 34.5 KJ/mole with the increase of $CO_2$ adsorption. For both adsorbents, the heat of $CO_2$ adsorption was increased after the minimum with an increase of $CO_2$ adsorption capacity. It was due to the heterogeneity of the adsorbent.

Adsorption stability of an adsorbent can be known by multiple adsorption cycles. Fig. 8(b) shows multiple $CO_2$ adsorption cycles of 10MgO/MC at 298 K. Before study of each adsorption cycle, the adsorbent was degasified at 473 K for 2 h under vacuum. 10MgO/MC showed constant $CO_2$ adsorption capacity up to five cycles. The $CO_2$ adsorption of 10MgO/PC was compared with some of the reported adsorbents (Table 3). The $CO_2$ adsorption capacity value was between the adsorption capacity of NiO supported on mesoporous carbon [16], iron oxide doped MCM-41 [15] and Zeolite-13X [32]. Hence, it is one of the adsorbents that has shown good adsorption capacity and selectivity.

## CONCLUSIONS

Mesoporous carbon and MgO incorporated mesoporous carbon samples were used as an adsorbent for the study of $CO_2$ capture and separation. The presence of MgO on mesoporous was confirmed by all characterization techniques. 10MgO/MC showed high adsorption of $CO_2$ 1.68 mmol/g at 298 K, 1 bar, which was higher than MC by electrostatic interaction between $CO_2$ and MgO. High selectivity of $CO_2$ over $N_2$ was 40 and heat of $CO_2$ adsorption was 36 KJ/mole at low coverage of $CO_2$ on 10MgO/MC. Stable $CO_2$ adsorption capacity was maintained in each adsorption cycle. Therefore, mesoporous carbon derived from pongamia pinnata fruit hulls can be used as an adsorbent and support to incorporate metal oxides to study $CO_2$ adsorption and separation.

## ACKNOWLEDGEMENT

HB and RA acknowledge the Science and Engineering Research

Board, Department of Science and Technology, New Delhi, India for the financial support (Grant No. EMEQ-283/2014).

## REFERENCES


1. S. Hosseini, I. Bayesti, E. Marahel, F. Eghbali Babadi, L. Chuah Abdullah and T. S. Y. Choong, *J. Taiwan Inst. Chem. Eng.*, **52,** 109 (2015).
2. D. Aaron and C. Tsouris, *Sep. Purif. Technol.*, **40**, 321 (2005).
3. M. K. Al Mesfer and M. Danish, *J. Environ. Chem. Eng.*, **6**, 4514 (2018).
4. R. Seabra, A. M. Ribeiro, K. Gleichmann, A. F. P. Ferreira and A. E. Rodrigues, *Micropor. Mesopor. Mater.*, **277**, 105 (2019).
5. J. Pires, M. Bestilleiro, M. Pinto and A. Gil, *Sep. Purif. Technol.*, **61**, 161 (2008).
6. C. Knöfel, J. Descarpentries, A. Benzaouia, V. Zeleňák, S. Mornet, P. L. Llewellyn and V. Hornebecq, *Micropor. Mesopor. Mater.*, **99**, 79 (2007).
7. B. B. Saha, S. Jribi, S. Koyama and I. I. El-Sharkawy, *J. Chem. Eng. Data*, **56**, 1974 (2011).
8. I. I. Gurten, M. Ozmak, E. Yagmur and Z. Aktas, *Biomass Bioenergy*, **37**, 73 (2012).
9. S. Rattanapan, J. Srikram and P. Kongsune, *Energy Procedia*, **138**, 949 (2017).
10. H. Deng, G. Li, H. Yang, J. Tang and J. Tang, *Chem. Eng. J.*, **163**, 373 (2010).
11. T. Uysal, G. Duman, Y. Onal, I. Yasa and J. Yanik, *J. Anal. Appl. Pyrolysis*, **108**, 47 (2014).
12. S. M. Yakout and G. Sharaf El-Deen, *Arabian J. Chem.*, **9**, S1155 (2016).
13. X. Zhao, W. Li, F. Kong, H. Chen, Z. Wang, S. Liu and C. Jin, *Mater. Chem. Phys.*, **219**, 461 (2018).
14. Y. Gao, L. Li, Y. Jin, Y. Wang, C. Yuan, Y. Wei, G. Chen, J. Ge and H. Lu, *Appl. Energy*, **153**, 41 (2015).
15. K. C. Chanapattharapol, S. Krachuamram and S. Youngme, *Micropor. Mesopor. Mater.*, **245**, 8 (2017).
16. M. Li, K. Huang, J. A. Schott, Z. Wu and S. Dai, *Micropor. Mesopor. Mater.*, **249**, 34 (2017).
17. B. J. Kim, K. S. Cho and S. J. Park, *J. Colloid Interface Sci.*, **342**, 575 (2010).
18. D. I. Jang and S. J. Park, *Fuel*, **102**, 439 (2012).
19. J. Shi, N. Yan, H. Cui, Y. Liu and Y. Weng, *J. Environ. Chem. Eng.*, **5**, 4605 (2017).
20. W. Cai, S. Zhang, X. Hu and M. Jaroniec, *Energy Fuels*, **32**, 9701 (2018).
21. H. Zhao, W. Yan, Z. Bian, J. Hu and H. Liu, *Solid State Sci.*, **14**, 250 (2012).
22. H. Jeon, Y. J. Min, S. H. Ahn, S.-M. Hong, J. S. Shin, J. H. Kim and K. B. Lee, *Colloids Surf., A*, **414**, 75 (2012).
23. M. A. Islam, S. Sabar, A. Benhouria, W. A. Khanday, M. Asif and B. H. Hameed, *J. Taiwan Inst. Chem. Eng.*, **74**, 96 (2017).
24. B. Chen, Z. Yang, G. Ma, D. Kong, W. Xiong, J. Wang, Y. Zhu and Y. Xia, *Micropor. Mesopor. Mater.*, **257**, 1 (2018).
25. S. J. Park and S. Y. Lee, *J. Colloid Interface Sci.*, **346**, 194 (2010).
26. S. Brunauer, P. H. Emmett and E. Teller, *J. Am. Chem. Soc.*, **60**, 309 (1938).
27. W. Tian, Q. Gao, Y. Tan, K. Yang, L. Zhu, C. Yang and H. Zhang, *J. Mater. Chem. A*, **3**, 5656 (2015).
28. S. Cheng, L. Zhang, H. Xia and J. Peng, *Green Process. Synth.*, **6**, 487 (2017).
29. M. Saleh, J. N. Tiwari, K. C. Kemp, M. Yousuf and K. S. Kim, *Environ. Sci. Technol.*, **47**, 5467 (2013).
30. C. Goel, H. Bhunia and P. K. Bajpai, *J. Environ. Chem. Eng.*, **4**, 346 (2016).
31. J. Yan, Y. Yu, C. Ma, J. Xiao, Q. Xia, Y. Li and Z. *Li, Appl. Therm. Eng.*, **84**, 118 (2015).
32. J. McEwen, J. D. Hayman and A. Ozgur Yazaydin, *Chem. Phys.*, **412**, 72 (2013).
33. K. Upendar, T. V. Sagar, G. Raveendra, N. Lingaiah, B. V. S. K. Rao, R. B. N. Prasad and P. S. S. Prasad, *RSC Adv.*, **4**, 7142 (2014).
34. S. Zhang, W. Cai, J. Yu, C. Ji and N. Zhao, *Chem. Eng. J.*, **310**, 216 (2017).